PROBLEMY TRANSPORTU

DOI: 10.20858/tp.2025.20.3.18

**Keywords:** vehicle stability; dynamic model; two axle vehicle

Rosen IVANOV<sup>1</sup>\*, Donka IVANOVA<sup>2</sup>, Georgi KADIKYANOV<sup>3</sup>, Gergana STANEVA<sup>4</sup>, Iliyana MINKOVSKA<sup>5</sup>

# THEORETICAL STUDY OF THE STABILITY OF A TWO-AXLE VEHICLE WITH A DYNAMIC MODEL

**Summary.** In this paper, the possibility of a more precise evaluation of critical speed is presented. A developed dynamic model of a two-axle vehicle is described and used. The work of the model is demonstrated with graphical results concerning one of the investigated cases of unsteady motion. The advantages and problems of the presented approach are analyzed.

### 1. INTRODUCTION

The undefined driving modes of a vehicle are difficult to describe and model. On the other hand, it is necessary to study traction properties, stability, maneuverability, etc. Models of the behavior of the vehicle and its systems have been developed by a number of authors and groups [1, 11].

In [3], a full model of vehicle steering using proportional-integral-differential (PID) control was developed. The idea was to reduce lateral slip and to improve stability. Simulations were done.

Lateral vehicle stability is considered in [4]. The authors studied the application of the active front wheel steering and individual braking to improve stability.

In the paper [5], a rear axle side slip angle controller is developed. The primary objective is to enhance the stability control of passenger cars in oversteer situations. The same problem is regarded in [6] for long heavy vehicles.

Active body control was studied in [7]. An impact force estimation method and a vehicle motion prediction scheme were proposed to characterize the vehicle motion after a crash event.

An improved method of obtaining lateral stability regions for road vehicles is presented in [8]. The method considers the influence of steering angle, center of gravity, longitudinal speed, and tire-road friction coefficient on the vehicle dynamics. Comprehensive stability regions are obtained for a wide range of such parameters.

In [9], a model of a four-wheel steering distributed drive vehicle is presented. The vehicle had independent control over the four-wheel angle and wheel torque. A method for jointly controlling the distribution of the wheel angle and torque was proposed, based on this characteristic.

A team, including the authors, developed a model for determining the normal reactions in the unsteady motion of a two-axle vehicle. A simulation model was implemented in the SIMULINK environment, and the first simulations were performed [1]. The model was subsequently further

<sup>&</sup>lt;sup>1</sup> University of Ruse; Studentska 8, 7017 Ruse, Bulgaria; e-mail: rossen@uni-ruse.bg; orcid.org/0000-0002-0573-4316

<sup>&</sup>lt;sup>2</sup> University of Ruse; Studentska 8, 7017 Ruse, Bulgaria; e-mail: divanova@uni-ruse.bg; orcid.org/0000-0002-6215-4203

<sup>&</sup>lt;sup>3</sup> University of Ruse; Studentska 8, 7017 Ruse, Bulgaria; e-mail: gkadikyanov@uni-ruse.bg; orcid.org/0000-0002-6215-4203

<sup>&</sup>lt;sup>4</sup> University of Ruse; Studentska 8, 7017 Ruse, Bulgaria; e-mail: glstaneva@uni-ruse.bg; orcid.org/0009-0003-0015-4149

<sup>&</sup>lt;sup>5</sup> University of Ruse; Studentska 8, 7017 Ruse, Bulgaria; e-mail: iminkovska@uni-ruse.bg; orcid.org/0009-0007-8348-0298

<sup>\*</sup> Corresponding author. E-mail: rossen@uni-ruse.bg

developed to also determine the lateral reactions, the traction force, and the total reactions on the wheels and on the axles, using friction ellipses.

This work aims to present the results obtained with the model and its capabilities for studying stability against lateral slip in the presence of acceleration/deceleration and longitudinal road inclination.

## 2. MODEL

The scheme of force, acting on a two-axle vehicle with a 4x2 wheel formula during uneven motion, in a turn with a variable radius, on a road with a longitudinal and lateral inclination, is shown in Fig. 1. The motion is accompanied by side slip of the vehicle tires, in which the center of the turn moves from p.  $O_1$  (when moving without lateral slip) to p.  $O_{\delta}$ . The radius of the turn is determined by the expression

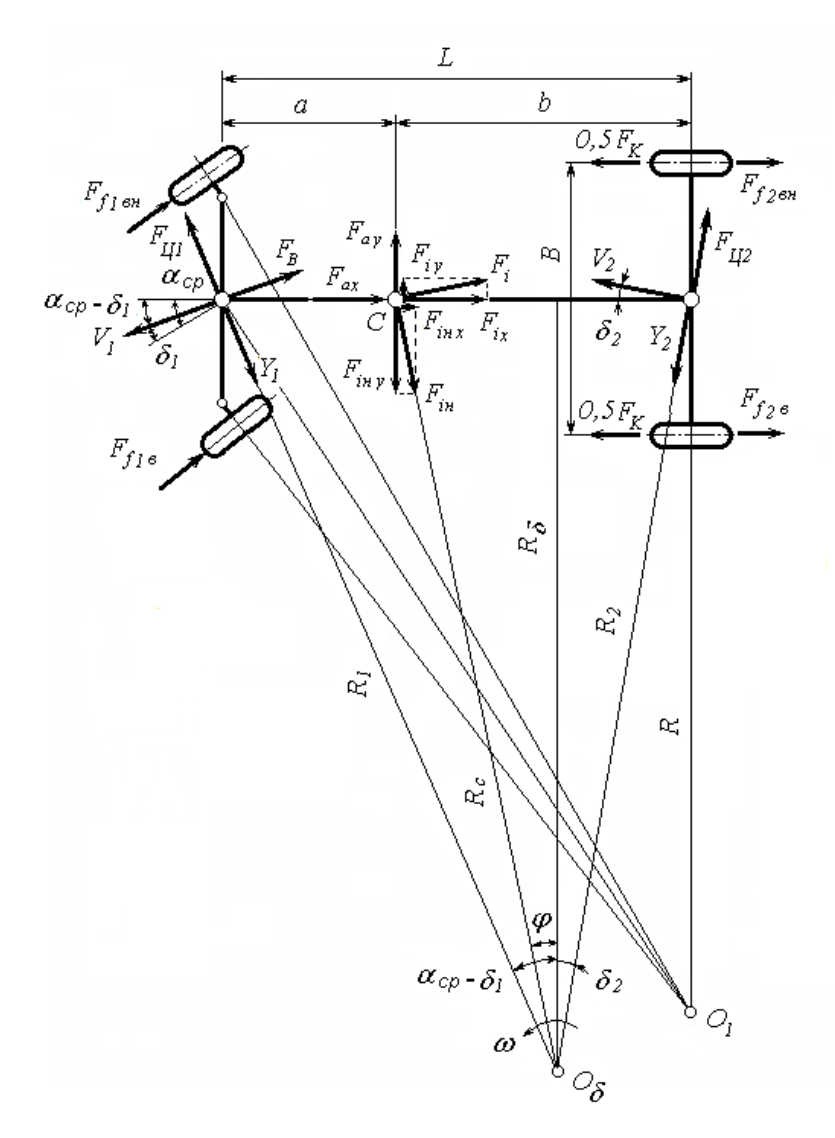


Fig. 1. Forces acting on a two-axle vehicle during the motion at variable speed and turning radius on a road with longitudinal and lateral inclination

$$R_{\delta} = \frac{L}{tg(\alpha_{\rm cp} - \delta_1) + tg\delta_2},\tag{1}$$

where  $\delta_1$  and  $\delta_2$  are the angles of side slip of the front and rear axles of the vehicle.

The radius from the center of the rotation  $O_{\delta}$  to the center of gravity of the car C is determined by the formula

$$R_c = \sqrt{R_\delta^2 + (b - R_\delta t g \delta_2)^2} , \qquad (2)$$

where b is the longitudinal coordinate of the car's center of gravity relative to its rear axle.

As in the previous model, when deriving the dependencies, the speed  $V_2$  of the rear axle is assumed to be the speed of the vehicle.

The forces  $F_{ax}$  and  $F_{ay}$ , which act during uneven motion along a curve with a variable radius, can be determined based on the longitudinal  $a_x$  and lateral accelerations  $a_y$  acting at the center of gravity of the car, point C (Fig. 2). These accelerations can be determined using the well-known approach described in [1], modified for a car with elastic tires, taking into account the lateral slip during motion along a curve.

The motion of the center of gravity point C (Fig. 2) around the center of the bend is considered as the sum of the rotation of point A around the center of the bend (translational motion) and the rotation of point C relative to point A in a translationally moving coordinate system (relative motion). The normal and tangential acceleration of point A during translational motion are expressed by the following dependencies:

$$a_A^n = \omega^2 R_\delta = \frac{V_2^2 \cos^2 \delta_2}{R_\delta},\tag{3}$$

$$a_A^t = \cos \delta_2 \frac{dV_2}{dt}. (4)$$

The normal and tangential acceleration of point C in relative motion are determined by the following expressions:

$$a_{CA}^{n} = b_{1} \frac{V_{2}^{2} \cos^{2} \delta_{2}}{R_{\delta}^{2}} = \frac{bV_{2}^{2} \cos^{2} \delta_{2}}{R_{\delta}^{2}} - \frac{V_{2}^{2} \cos^{2} \delta_{2} tg\delta_{2}}{R_{\delta}},$$
 (5)

$$a_{CA}^{n} = b_{1} \frac{v_{2}^{2} \cos^{2} \delta_{2}}{R_{\delta}^{2}} = \frac{b v_{2}^{2} \cos^{2} \delta_{2}}{R_{\delta}^{2}} - \frac{v_{2}^{2} \cos^{2} \delta_{2} t g \delta_{2}}{R_{\delta}},$$

$$a_{CA}^{t} = \frac{b_{1}}{L} \left[ \left( \cos \delta_{2} t g \left( \alpha_{cp} - \delta_{1} \right) + \sin \delta_{2} \right) \frac{d v_{2}}{dt} + \frac{v_{2} \cos \delta_{2}}{\cos^{2} \left( \alpha_{cp} - \delta_{1} \right)} \frac{d \alpha_{cp}}{dt} \right].$$
(6)

Taking into account (3)–(6) and the fact that  $b_1 = b - R_{\delta} \tan \delta_2$ , the longitudinal and lateral acceleration acting at the center of gravity of the car point C are determined by

$$a_{x} = a_{A}^{t} - a_{CA}^{n} = \cos \delta_{2} \frac{dV_{2}}{dt} - \left(\frac{bV_{2}^{2}\cos^{2}\delta_{2}}{R_{\delta}^{2}} - \frac{V_{2}^{2}\cos \delta_{2}\sin \delta_{2}}{R_{\delta}}\right),\tag{7}$$

$$a_{x} = a_{A}^{t} - a_{CA}^{n} = \cos \delta_{2} \frac{dV_{2}}{dt} - \left(\frac{bV_{2}^{2}\cos^{2}\delta_{2}}{R_{\delta}^{2}} - \frac{V_{2}^{2}\cos \delta_{2}\sin \delta_{2}}{R_{\delta}}\right), \tag{7}$$

$$a_{y} = a_{A}^{n} + a_{CA}^{t} = \frac{V_{2}^{2}\cos^{2}\delta_{2}}{R_{\delta}} + \frac{b - R_{\delta}tg\delta_{2}}{L} \left[ \left(\cos \delta_{2} tg(\alpha_{cp} - \delta_{1}) + \sin \delta_{2}\right) \frac{dV_{2}}{dt} + \frac{V_{2}\cos \delta_{2}}{\cos^{2}(\alpha_{cp} - \delta_{1})} \frac{d\alpha_{cp}}{dt} \right] \tag{8}$$

The longitudinal  $F_{ax}$  and lateral forces  $F_{ay}$  resulting from the uneven motion in a curve with a variable radius can be determined by  $a_x$  and  $a_y$ :

$$F_{ax} = a_x \delta_a m,$$
 (9)  
$$F_{ay} = a_y m,$$
 (10)

$$F_{av} = a_v m, (10)$$

where m is the mass of the car and  $\delta_a$  is the coefficient of influence of rotating masses.

The resistance from the longitudinal inclination of the road (Figs. 3 and 4)  $F_i = G \sin \alpha_{H} \cos \beta$  is decomposed into two components:

$$F_{ix} = F_i \cos \phi = G \sin \alpha_{\rm H} \cos \beta \cos \phi; \qquad F_{iy} = F_i \sin \phi = G \sin \alpha_{\rm H} \cos \beta \sin \phi. \tag{11}$$

The lateral forces in the front and rear axles of the vehicle, caused by the resistance to the inclination, taking into account the distribution of masses, are

$$F_{iy1} = \frac{Gb}{L} \sin \alpha_{\rm H} \cos \beta \sin \phi;$$
  $F_{iy2} = \frac{Ga}{L} \sin \alpha_{\rm H} \cos \beta \sin \phi.$  (12)  
The resistance from the lateral inclination of the road (Fig. 4)  $F_{i_H} = G \sin \beta \cos \alpha_{\rm H}$  is decomposed

into two components:

$$F_{iH_{\chi}} = G \sin \beta \cos \alpha_H \sin \phi;$$
  $F_{iH_{\chi}} = G \sin \beta \cos \alpha_H \cos \phi.$  (13)

The lateral force in the front and rear axles of the car, caused by the lateral inclination (Fig. 4), is

$$F_{i_{\rm H}y_1} = \frac{Gb}{L} \sin\beta \cos\alpha_{\rm H} \cos\phi, \qquad F_{i_{\rm H}y_2} = \frac{Ga}{L} \sin\beta \cos\alpha_{\rm H} \cos\phi. \tag{14}$$

The angle  $\varphi$  that y participates in (11)-(14) can be determined from the following dependencies:

$$\cos\phi = \frac{R_\delta}{\sqrt{(b-R_\delta t g \delta_2)^2 + R_\delta^2}} \text{ and } \sin\phi = \frac{b-R_\delta t g \delta_2}{\sqrt{(b-R_\delta t g \delta_2)^2 + R_\delta^2}}.$$
 If the lateral components of  $F_{f2}$ ,  $F_B$ , and  $F_{f1}$  are neglected due to their small values, for the front

and rear axles, the lateral forces are

$$F_{y1} = \frac{Gb}{L} \left( \frac{a_y}{g} \cos \beta + \sin \alpha_H \sin \phi \cos \beta - \sin \beta \cos \alpha_H \cos \phi \right), \tag{15}$$

$$F_{y2} = \frac{Ga}{L} \left( \frac{a_y}{a} \cos \beta + \sin \alpha_{_H} \sin \phi \cos \beta - \sin \beta \cos \alpha_{_H} \cos \phi \right). \tag{16}$$

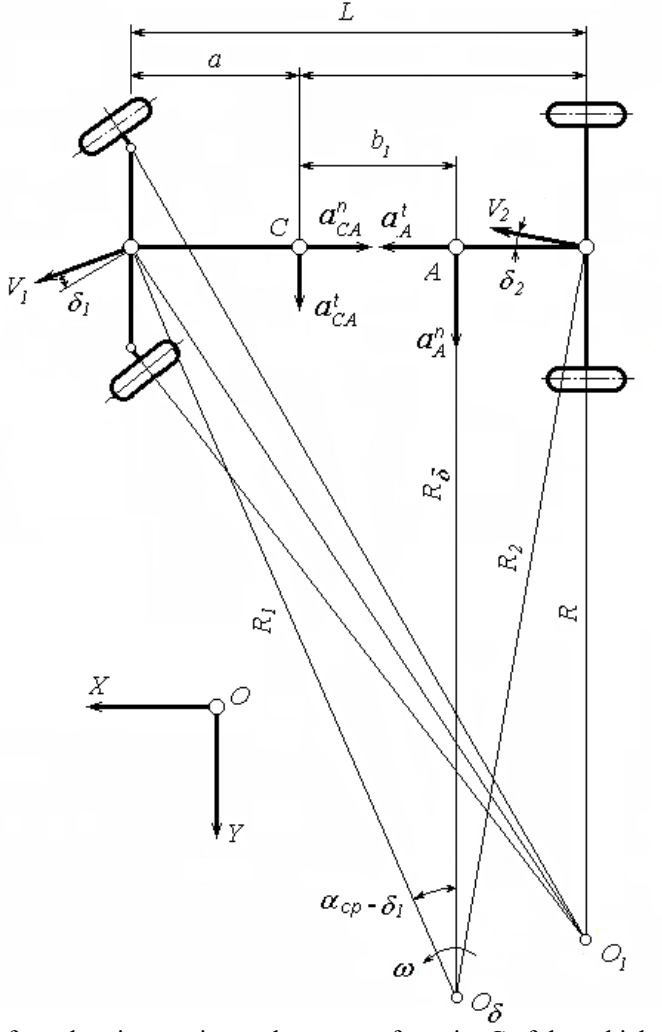


Fig. 2. Determination of accelerations acting at the center of gravity C of the vehicle

The normal load is redistributed between the front and rear axles of the vehicle under the action of the longitudinal components of the inertial force, the resistance from the longitudinal and lateral inclination of the road, and the air resistance (Fig. 3). For the normal reactions on the front and rear wheels, we obtain, respectively

$$Z_1 = \frac{\overline{(G\cos\beta + F_{ay}\sin\beta)}}{I}(b\cos\alpha_{\rm H} + fr_k\cos\alpha_{\rm H} - D), \tag{17}$$

$$Z_2 = \frac{(G\cos\beta + F_{ay}\sin\beta)}{r} (a\cos\alpha_{\rm H} - fr_k\cos\alpha_{\rm H} + D), \tag{18}$$

$$Z_{1} = \frac{(G\cos\beta + F_{ay}\sin\beta)}{L} (b\cos\alpha_{H} + fr_{k}\cos\alpha_{H} - D),$$

$$Z_{2} = \frac{(G\cos\beta + F_{ay}\sin\beta)}{L} (a\cos\alpha_{H} - fr_{k}\cos\alpha_{H} + D),$$

$$D = \frac{h}{g} (g\sin\alpha_{H}\cos\phi + g\tan\beta\cos\alpha_{H}\sin\phi + \frac{a_{x}\delta_{a}}{\cos\beta} + \frac{gk_{B}SV_{2}^{2}}{G\cos\beta}),$$

$$(19)$$

where: f – the coefficient of resistance to motion of the vehicle;

 $r_k$  – the radius of the car's wheels;

h – the height of the car's center of gravity (it is assumed that the force  $F_R$  is applied at the same height);

 $k_B$  – the air resistance coefficient;

S – the frontal area of the car.

The angle  $\alpha_{H}$  of the road inclination has a positive sign when climbing and a negative sign when descending.

Under the action of the lateral forces on the front and rear axles, the outer wheels of the vehicle relative to the center of the bend are loaded, and the inner wheels are unloaded. From Fig. 4, the following relationships are obtained for the normal reactions acting on the outer and inner wheels

$$Z_{1B,1BH} = \frac{Z_1}{2} \mp \frac{F_{y_1}h}{R},\tag{20}$$

$$Z_{1B,1BH} = \frac{Z_1}{2} \mp \frac{F_{y_1}h}{B},$$

$$Z_{2B,2BH} = \frac{Z_2}{2} \mp \frac{F_{y_2}h}{B},$$
(20)

where B is the lateral base of the car.

The upper signs in Formulas (20) and (21) refer to the inner, and the lower signs to the outer front and rear wheels with respect to the center of the turn.

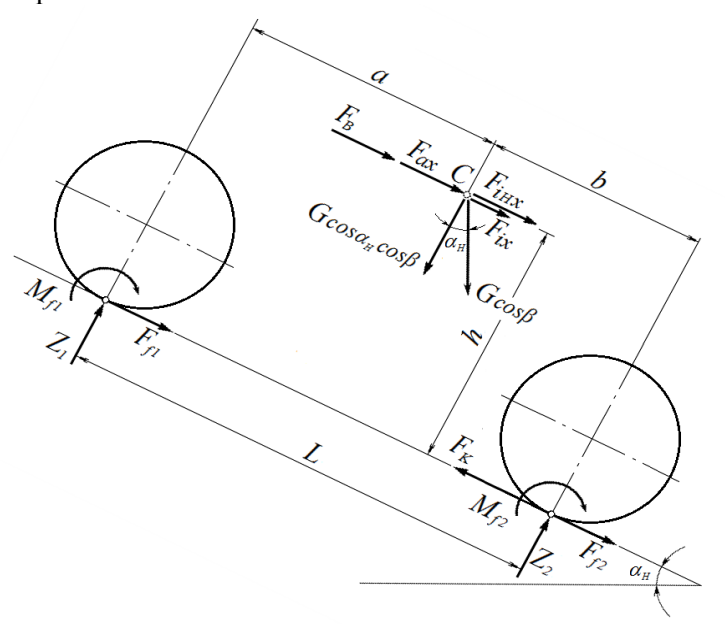


Fig. 3. Diagram of forces acting on a two-axle vehicle climbing a slope

The lateral slips of the wheels are needed to evaluate lateral reactions; they can be found sequentially with iterations, initially assuming that they are equal to zero. For the second iteration, the calculated slips are used with the results of the lateral reactions from the first, etc. As soon as the difference between the results of two consecutive iterations is small enough (less than 0.5%), the calculations can be terminated. It should also be taken into account that with paired wheels in the rear axle of some trucks, the lateral stiffness is twice as large, and this must be taken into account when determining the slip angles. In the iterative process for determining the lateral slip angles and the lateral reactions of the wheels, the method described by K. Enke can be used, taking into account the experimental characteristics of the tires when rolling with lateral slip  $\delta = f(Y)$  for different wheel loads. The theoretical approach and dependencies can also be used [1, 10].

The longitudinal reactions in the contact zone between the wheels and the road in different driving modes can be calculated by taking into account the acting traction and braking forces in each respective case of motion. The new feature of the current model is that braking forces can be determined using the longitudinal acceleration of the center of gravity, as calculated by the model. For the braking forces, dependency can be used, related to the axles.

$$F_{\alpha x 1} = a_x \delta_{\alpha} Z_1 / g, \tag{22}$$

$$F_{ax_2} = a_x \delta_a Z_2 / g \tag{23}$$

 $F_{ax1} = a_x \delta_a Z_1/g, \tag{22} \\ F_{ax_2} = a_x \delta_a Z_2/g \tag{23} \\ \text{Through the obtained longitudinal and lateral reactions, the magnitude of the resultant reaction } R_i$ (Fig. 5) at the contact between each wheel and the road can be found using the formula

$$R_i = \sqrt{X_i^2 + Y_i^2} \,, \tag{24}$$

where the forces at the places of Xi and Yi can be displaced as total longitudinal Fx and lateral Fy forces for each wheel.

Through the adhesion ellipses, an assessment of the exhaustion of adhesion on each wheel and on the axles can be made, in the manner explained in the previous point. If the resultant reaction  $R_i$  for a given wheel does not go outside the friction ellipse corresponding to the specific air pressure in the tires, the normal load, and the inclination of the wheel, then the resultant reaction does not exceed the adhesion force, and there is no danger of loss of adhesion for this wheel. The adhesive force  $F\varphi$  is determined from the experimentally obtained ellipse of adhesion (see p. A on Fig. 5)

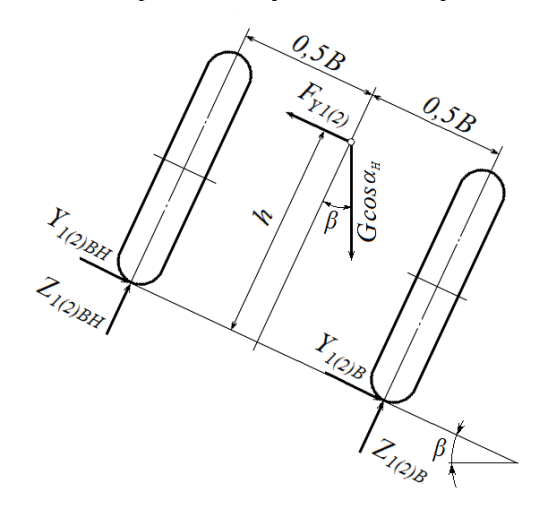


Fig. 4. Diagram of forces acting on a two-axle vehicle during motion on a lateral inclination

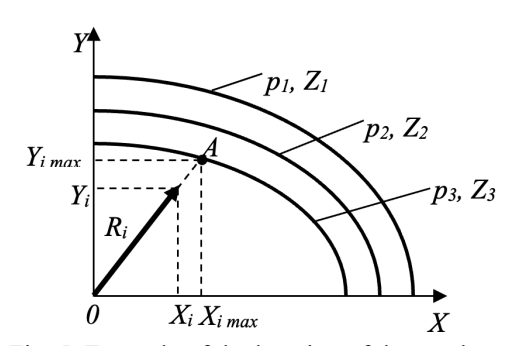


Fig. 5. Example of the location of the resultant reaction  $R_i$  in the area of the ellipses of adhesion:  $p_{1,2,3}$  – different tire pressures;  $Z_{1,2,3}$  – different vertical reactions on the tire

## Model capabilities

The described model can determine the resultant reaction in the contact patch and the traction force with the road for each tire for the general case of unsteady motion of a two-axle vehicle. Thus, it is possible to study the change in traction of each wheel and the entire vehicle, as well as the danger of loss of traction in each specific case of motion.

For the most general case of unsteady motion with variable acceleration/deceleration, in a curve with a variable radius, on a road with a longitudinal and lateral inclination and various special cases thereof (such as braking in a curve with a constant radius, acceleration or braking on a slope on a straight section of the road, braking in a curve with a variable radius on a horizontal section, etc.), the redistribution of the normal reactions of the wheels and their influence on the braking properties and the resistance to slip of the two-axle machine under consideration can be theoretically studied.

The model can be used to determine the critical speed  $V_{cr}$  of the vehicle against slipping. The critical speed is taken to be the speed at which one of the two axles of the vehicle loses grip. The loss of grip occurs when the resultant reaction exceeds the adhesion force, as described above.

To facilitate the work with the model and perform the voluminous calculations, a computer program was developed in the SIMULINK environment. The model allows for the simulation of all reactions on axles as a function of time during unsteady motion. It was used in conducting theoretical studies with this model. The input data of the program are the bases of the vehicle L and B; average steering angle  $\alpha_{cp}$  of the wheels; speed V; and some other constants like vehicle weight. The output results include a graph of the resulting reactions on axles R1 and R2, as well as the adhesion forces on axles  $F\varphi_1$  and  $F\varphi_2$ .

For theoretical studies with the developed model, it is necessary to have experimental data on the influence of normal load, tire pressure, and wheel inclination angle on the coefficients of adhesion in the lateral and longitudinal directions and the coefficient of resistance against lateral slip, as well as for some other quantities. For them, regression relationships should be developed for the influence of the listed operational factors.

# 3. ANALYTICAL STUDY OF THE STABILITY AGAINST LATERAL SLIP OF A TWO-AXLE VEHICLE IN DIFFERENT CASES OF UNSTABLE MOTION

The purpose of the analytical study at this point is to assess the capabilities of the model and examine its robustness against slipping.

The model uses experimental values obtained during testing of a truck tire model 11.00R20, such as the adhesion coefficient  $\varphi$ , the lateral slip coefficient k  $\delta$ , and their dependence on the load and air pressure in the tires.

The geometric and mass parameters used in the simulations are taken from a real two-axle truck with twin tires on the rear axle. The main ones are:

- full weight -160 kN;
- − longitudinal base − 5.0 m;
- distance from the center of gravity to the rear axle -1.875 m;
- lateral base -B = 2.25 m;
- frontal area  $S = 7.4 \text{ m}^2$ ;
- air resistance coefficient  $k_B = 0.6 \text{ Ns}^2/\text{m}^4$ ;
- height to the center of gravity -h = 1.5 m;
- wheel radius  $r_k = 0.505$  m;
- rolling resistance coefficient f = 0.018;
- initial value of the adhesion coefficient  $\varphi = 0.6/0.8/0.85$

For this purpose, several cases of motion were studied:

Case 1: Motion in a curve with constant radius and constant speed of motion (R = const, V = const);

Case 2: Braking in a curve with a constant radius and constant braking deceleration (R = const, V = var,  $a_{\sigma\pi} = const$ );

Case 3: Straight-line stopping with constant deceleration ( $R = \infty$ , V = var,  $a_{cn} = const$ );

Case 4: Motion in a curve with variable radius and constant speed (R = var, V = const);

Case 5: Driving in a curve with variable radius, variable speed, and constant braking deceleration  $(R = var, V = var, a_{cn} = const)$ ;

Case 6: Driving in a curve with variable radius, variable speed, and variable braking deceleration  $(R = var, V = var, a_{cp} = var)$ ;

Case 7: Motion in a curve with variable radius, variable speed, and constant acceleration (R = var, V = var, a = const):

Case 8: Motion in a curve with variable radius, variable speed, and variable acceleration (R = var, V = var, a = var).

For all the mentioned cases of motion, graphical dependences of the change in the average angle of the steered wheels  $\alpha_{cp}$  have been obtained, the radius of the turn  $R_{\delta}$ , the speed of motion  $V_2$ , the normal  $Z_i$ , the lateral  $F_{Yi}$ , and the longitudinal  $F_{Xi}$  reactions on the wheels, the adhesion force  $F_{\varphi i}$  and the total reactions  $R_i$  on axles.

For each of the studied cases, six graphs were obtained. Each graph combined and displayed several quantities over time in an appropriate manner. Due to the inability to display some symbols in the programming environment, some quantities are not displayed in the legends of the figures, as in the mathematical relationships.

Because of the limitation of the pages, in this publication, only the results for the seventh studied case are shown as an example in Figs. 6–11. The results for all cases are summarized in Table 1.

## 3.1. Analysis of the results

The results (Figs. 6–11) show that all reactions acting on the wheels of a two-axle truck under complex unsteady driving modes can be simulated.

From the figures showing the total reactions and the adhesion force on the axles, the vehicle's resistance to lateral slip can be assessed. For example, for the seventh case in Figs. 10 and 11, it can be seen that there is a time interval in which the total reaction on the axles exceeds the adhesion force, which means that there is slipping of the axles. From the intersection points of the total reaction and the adhesion force, it can be determined at what point in time the loss of stability occurred (see dash lines), and from the corresponding graphs for speed changes (Fig. 6), it can be determined what the speed value was at that same moment (see also dash lines). It is critical to prevent the slipping of some of the axles and loss of lateral stability by the vehicle. In this way, the critical speed can be determined in each specific case of motion. The dashed lines in Figs. 6, 10, and 11 are added only to illustrate the methodology. The SIMULINK model does this automatically and gives the final result as critical speed *Vcr m* (illustrated at Fig. 6, for example)

From Figs. 7, 8, 10, and 11, some shortcomings of the model are also visible – at certain values of the input quantities, interruptions occur in the graphs. For example, at a wheel slip angle of 0 degrees, due to uncertainty in the change of its sign, unnatural peaks are obtained (about the eighth second ). Similar peaks were also obtained at the initial moment, which are due to transient modes at the beginning of integration with the software product. Peaks in similar situations were obtained in the simulations and in the other cases of motion. A similar problem occurs when the entrainment of the axles  $\delta 1$  and  $\delta 2$  is the same.

The critical speed for a given case of motion is determined by the resulting graphical dependencies as follows. If the total reaction on an axle exceeds the adhesion force, this means that there is slipping on this axle. From the intersection points of the total reaction and the adhesion force, it is determined at what moment in time the loss of stability occurred. For the front axle (Fig. 10), it is moment t1, and for the rear axle, it is moment t2. From the corresponding graph of speed change over time (Fig. 6), the speed value is calculated at that same moment. It is the critical speed at which the vehicle slips and loses stability. Finally, the lower of the two values of the axles is accepted as the critical speed.

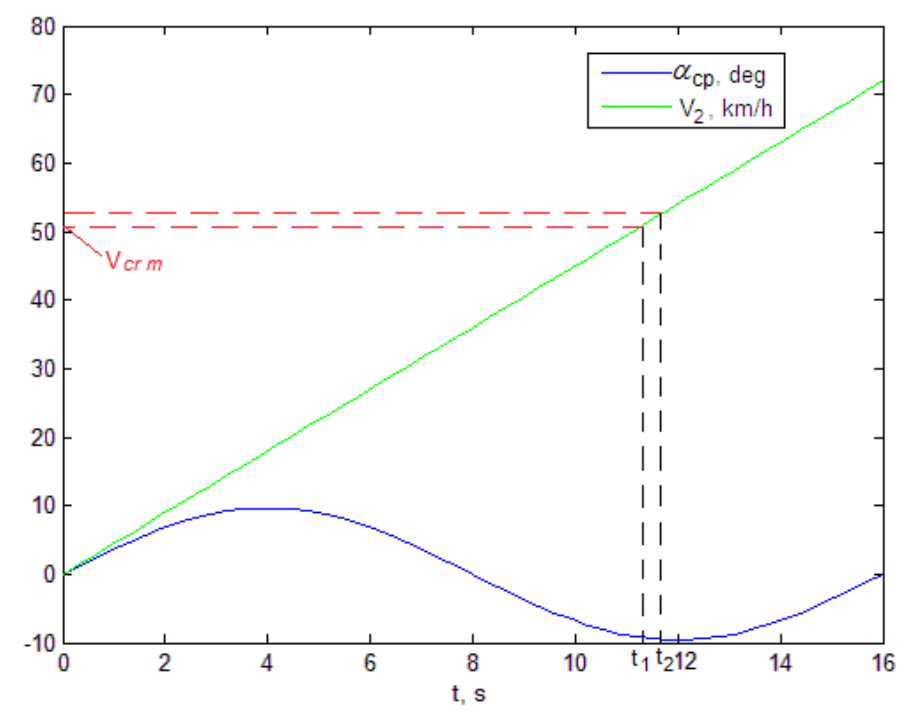


Fig. 6. Change in the average steering angle of the front wheel  $\alpha_{cp}$  and the speed of motion  $V_2$  in the seventh studied motion case

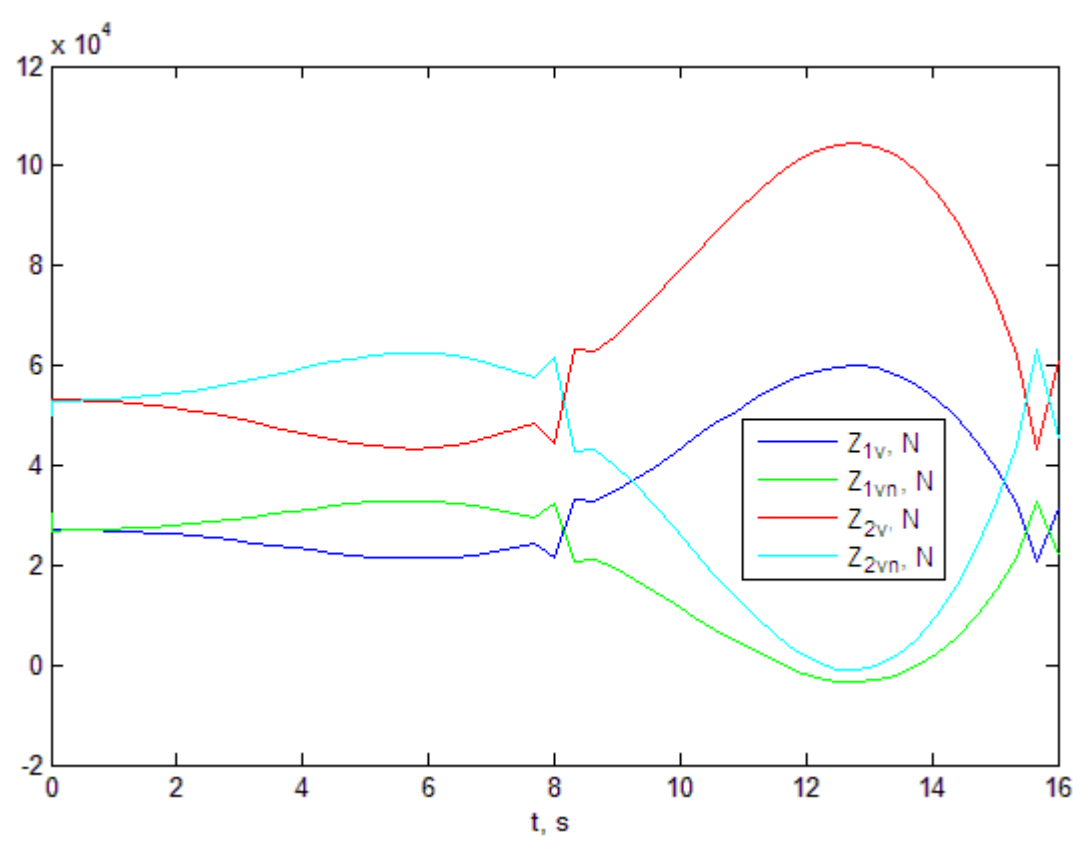


Fig. 7. Change in normal reactions on the wheels  $Z_i$  in the seventh case of motion

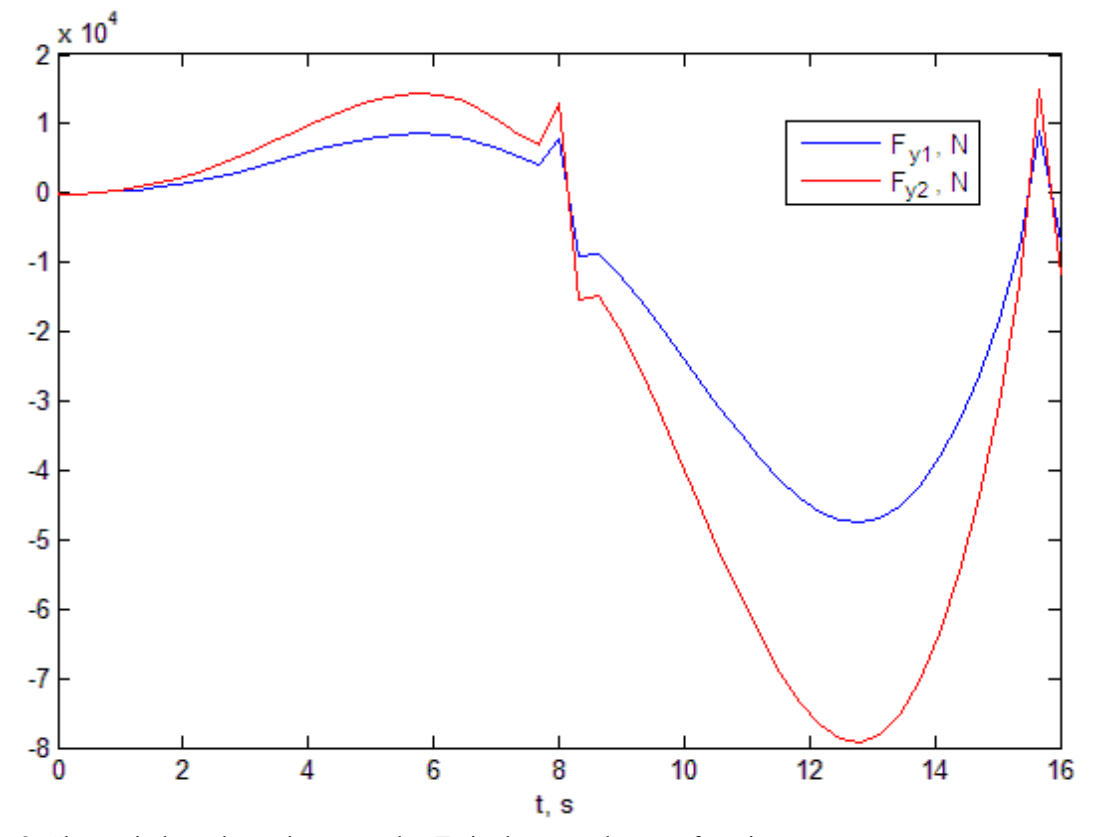


Fig. 8. Change in lateral reactions on axles  $F_{Yi}$  in the seventh case of motion

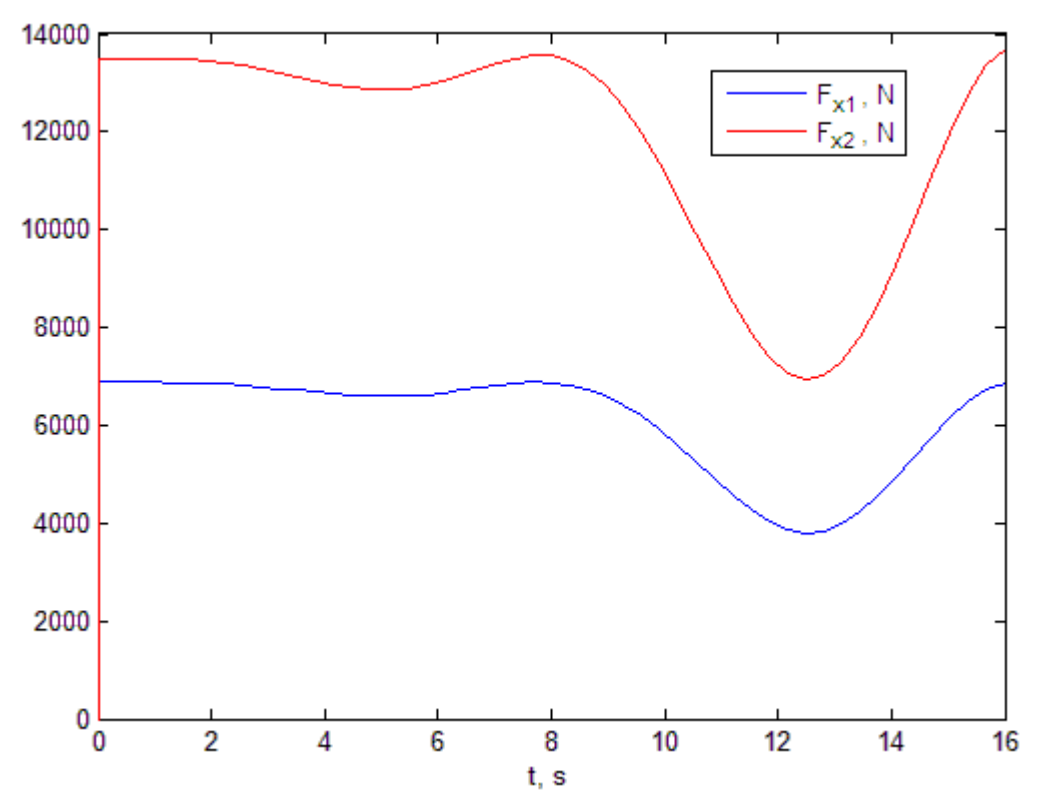


Fig. 9. Change longitudinal reactions on axles  $F_{Xi}$  in the seventh case of motion

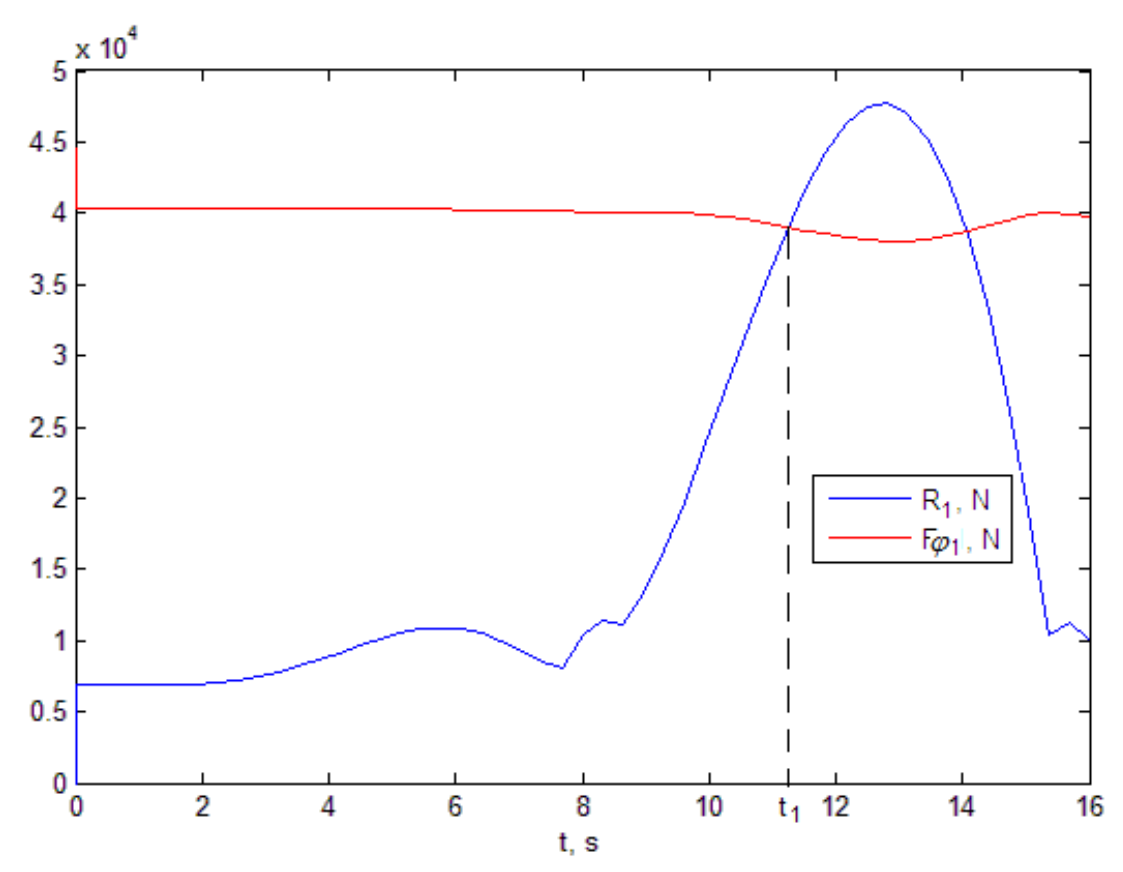


Fig. 10. Change the total reaction  $R_I$  and the adhesion force  $F_{\varphi iI}$  for the front axle in the seventh case of motion

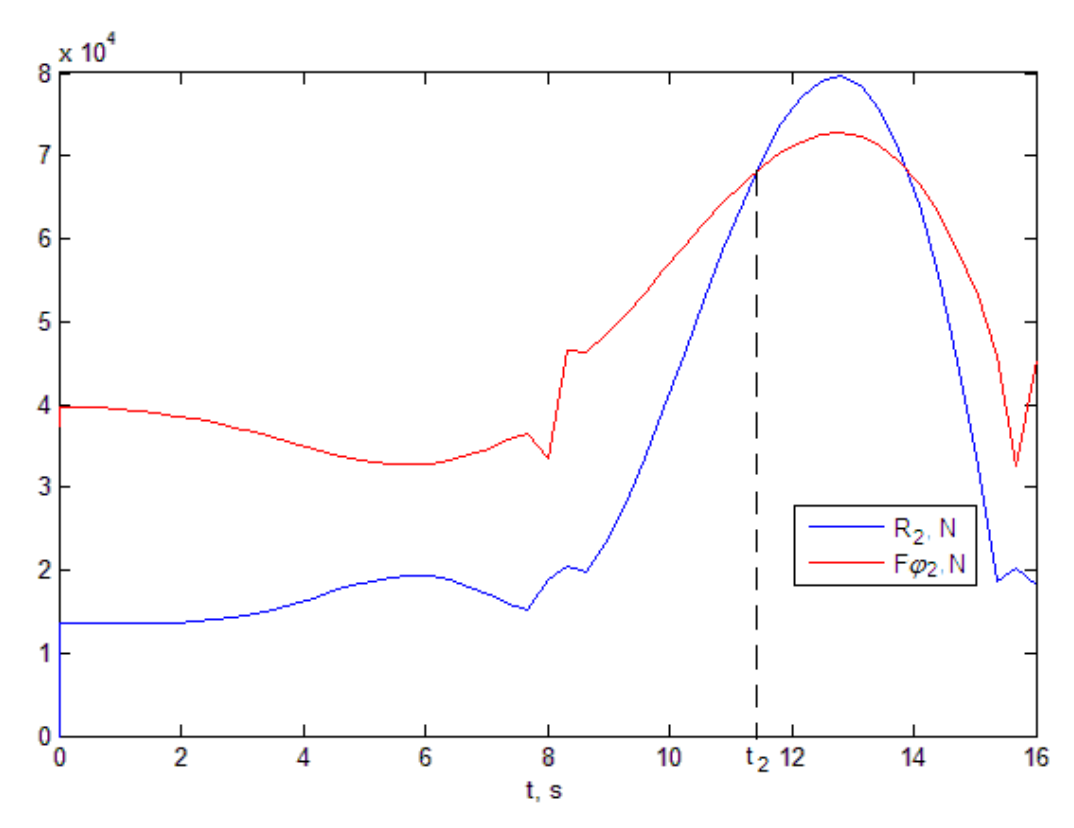


Fig. 11. Change the total reaction  $R_2$  and the adhesion force  $F_{\varphi 2}$  for the rear axle in the seventh motion case

The results in Table 1 summarize the findings for all studied cases of motion. The main indicators of motion are presented in the table. The critical speed in different cases is marked in red. In some cases, slipping did not occur.

## 4. CONCLUSIONS

The results obtained with the developed model and its software implementation can be used to study the vehicle's resistance to slip. They are more precise than the classical methodology because they take into account the redistribution of reactions and the change in the coefficient of adhesion.

The differences between the determined critical speed against slip by the model and the classical dependence [11] for the eight cases initially included in this study ranged from 6.05-7.92 km/h or 10.44-13.92%.

It has been established that the braking deceleration has a significantly stronger effect on the value of the critical speed than the longitudinal inclination of the road. At a braking deceleration of -6  $\text{m/s}^2$ , the reduction of the calculated critical speed compared to that determined by the classical methodology reached 40.75%.

The results also show some shortcomings of the model. At certain values of the input quantities, interruptions occur in the graphs. For the studied case, for example, at a wheel deflection angle equal to 0 degrees, due to uncertainty, unnatural peaks occurred (around the eighth second).

Similar peaks were also obtained at the initial moment of simulation. Peaks in similar situations were obtained in the simulations and in the other motion cases. Problems also emerge when the slip on the axles is the same.

Overall, despite these problems, the simulation model works well and determines the changes in response during complex driving modes for the two-axle vehicle.

As shown, it can be used to determine the critical speed and to study the resistance to slip. Future refinements to the model should aim to eliminate the identified shortcomings.

Table 1 Some motion parameters for the studied cases and theoretically determined critical speeds against lateral slip at  $\varphi_y = 0.8$ 

	_									_
Case 8	Rear	-/-	28,1	Acceleration, V = 0.54  km/h (sine wave)	-	Not reachable	Not reachable	55,24	ı	-
	Forv.				-	Not reachable	Not reachable	55,24	1	-
Case 7	Rear	-9,28 / -9,63	28,1	$a = +1,25$ $V = 0 \div 54 \text{ km/h}$	11,76	14,70	52,92	55,24	2,32	4,20
	Forv.				11,24	14,15	50,94	55,24	4,30	7,78
Case 6	Rear	LS*6 / -	∞→28,6	Breaking, V- sine wave	4,3	13,7	49,37	55,24	5,87	10,63
	Forv.				-	-	-	55,24	,	-
Case 5	Rear	9,62 / 9,11	∞→28,6	-1,25	4,9	13,95	50,22	55,24	5,02	60'6
	Forv.				4,4	14,60	52,56	55,24	2,68	4,85
Case 4	Rear	Drifting at $\alpha_{co}$ =9,57/9,40	∞→28,6	0	8,5	14,00 constant speed	50,40	55,24	-	-
Č	Forv.	Driftin =9,57	<b>↑</b> 8	)	9,1	14,00 constant speed	50,40	55,24	-	,
Case 3	Rear	0	8	Drifting at $a=6,95$	-	-	-	55,24	-	-
	Forv.				-	-	-	55,24		1
Case 2	Rear	94.6	28,6	-1	2,4	13,6	48,96	55,24	6,28	11,37
	Forv.				1,6	14,4	51,84	55,24	3,40	6,15
Case 1	Rear	9,46	28,6	0	1	14,1	50,76	55,24	4,48	8,11
	Forv.				-	-	-	55,24		1
Indicator	Axle	$a_{cp}$ , deg	$R_\delta$ , m	Acceleration / deseleration a , m/s²	Moment of occurrence of drift t, s	$V_{crm}$ , m/s (model)	$V_{crm}$ , km/h (model)	$V_{cr}$ , km/h (clasic, $\boldsymbol{\varphi}_{r}$ =0,8)	Difference, km/h	Difference, %

### References

- 1. Ivanov, R. & Avramov, E. & Ivanova, D. Modeling of the responses and study of the stability of a two-axle truck during unsteady motion. *Bultrans Proceedings*. Sofia. 2013. P. 58-63.
- 2. Sun, F.C. & My, B. & Chen, Sz. *Monitoring of Longitudinal Friction Characteristics Between Tire and Road Surface*. Beijing Institute of Technology. China. 2003.
- 3. Fachrudin & Robandi, I. & Sutantra, N. Model and simulation of vehicle lateral stability control. In: 2nd APTECS International Seminar on Applied Technology, Science, and Arts. ITS Surabaya. 2010.
- 4. Emirler, M.T. & Güvenç, B.A. *Model Predictive Vehicle Yaw Stability Control via Integrated Active Front Wheel Steering and Individual Braking*. MEKAR Mechatronics Research Lab, Mechanical Engineering Department, İstanbul Technical University, Turkey. DOI: 10.48550/arXiv.2210.10225.
- 5. Billmark, J. & Östh, J. Design and Evaluation of Rear Axle Side Slip Stability Control for Passenger Cars Simulations and Experimental Verification of Interventions in Oversteer Situations. Master's Thesis in Automotive Engineering. Department of Applied Mechanics, Division of Vehicle Safety, Chalmers University of Technology, Göteborg, Sweden. 2007.
- 6. Emheisen, M.A. & Emirler, M.T. & Basar, O. Lateral Stability Control of Articulated Heavy Vehicles Based on Active Steering System. *International Journal of Mechanical Engineering and Robotics Research.* 2022. Vol. 11. No. 8. P. 575-582.
- 7. Kim, B. & Peng, H. *Vehicle Stability Control of Heading Angle and Lateral Deviation to Mitigate Secondary Collisions*. University of Michigan. Available at: https://huei.engin.umich.edu/wp-content/uploads/sites/186/2015/02/AVEC12-Kim.pdf.
- 8. Alves, J.A.V. & Chinelato, C.I.G. & Angelico, B.A. Vehicle lateral stability regions for control applications. *IEEE Access*. 2017. Vol. 10. P. 87787-87802.
- 9. Zhang, J. & Liu, C. & Zhao, J. & Liu, H. Research on stability control of distributed drive vehiclewith four-wheel steering. *World Electr. Veh. J.* 2024. Vol. 15(6). No. 228.
- 10. Иванов, Р. Изследване устойчивостта на движение и износването на гумите на автомобилите. [In Bulgarian: Ivanov R. Study the vehicle stability and tires wear]. DSc dissertation, University of Ruse. 2014.
- 11. Gilespie, T.D. Fundamentals of Vehicle Dynamics. SAE. 1992.

Received 02.05.2024; accepted in revised form 27.08.2025